INTERNATIONAL JOURNAL FOR NUMERICAL METHODS IN FLUIDS
Int. J. Numer. Meth. Fluids 2003; **41**:47–75 (DOI: 10.1002/fld.428)

A convergent and universally bounded interpolation scheme for the treatment of advection

M. A. Alves[1,†], P. J. Oliveira[2,*,‡] and F. T. Pinho[3,§]

[1] *Departamento de Engenharia Química, Faculdade de Engenharia da Universidade do Porto, Rua Roberto Frias, 4200-465 Porto, Portugal*
[2] *Departamento de Engenharia Electromecânica, Universidade da Beira Interior, 6201-001 Covilhã, Portugal*
[3] *Centro de Estudos de Fenómenos de Transporte, DEMEGI, Faculdade de Engenharia da Universidade do Porto, Rua Roberto Frias, 4200-465 Porto, Portugal*

SUMMARY

A high resolution scheme with improved iterative convergence properties was devised by incorporating total-variation diminishing constraints, appropriate for unsteady problems, into an implicit time-marching method used for steady flow problems. The new scheme, referred to as Convergent and Universally Bounded Interpolation Scheme for the Treatment of Advection (CUBISTA), has similar accuracy to the well-known SMART scheme, both being formally third-order accurate on uniform meshes for smooth flows. Three demonstration problems are considered: (1) advection of three scalar profiles, a step, a sine-squared, and a semi-ellipse; (2) Newtonian flow over a backward-facing step; and (3) viscoelastic flow through a planar contraction and around a cylinder. For the case of the viscoelastic flows, in which the high resolution schemes are also used to represent the advective terms in the constitutive equation, it is shown that only the new scheme is able to provide a converged solution to the prescribed tolerance.

KEY WORDS: high resolution scheme (HRS); TVD property; boundedness; iterative convergence; viscoelastic fluids; CUBISTA

1. INTRODUCTION

One key issue in the numerical simulation of fluid flow problems is the representation of the first-derivative advection terms, which are invariably present in the governing equations. The question is not only how to devise a scheme with sufficient accuracy but, equally important, how to ensure that numerical stability is not diminished at the expense of increased accuracy. It is now well established [1] that the first-order upwind differencing scheme (UDS) and related schemes, like the HYBRID [2] and POWER-LAW [3], although highly stable are inadequate

* Correspondence to: P. J. Pimentel de Oliveira, Departamento de Engenharia Electromecânica, Universidade da Beira Interior, 6201-001 Covilhã, Portugal.
† E-mail: mmalves@fe.up.pt
‡ E-mail: pjpo@ubi.pt
§ E-mail: fpinho@fe.up.pt

Received 1 July 2001
Revised 13 August 2002

in that excessive numerical diffusion is generated in practical problems. Differencing schemes of order higher than unity are therefore required. Second-order accuracy can be achieved by linear extrapolation from two upstream values, yielding the so-called linear upwind scheme (LUDS), also known as second-order upwind, e.g. Reference [4]. Third-order is achieved by passing a quadratic line through those two upstream points and one downstream, the QUICK scheme of Leonard [5]. These schemes have been widely used [4–6] and generally offer more accurate results than upwind but, because they are not bounded, may give rise to oscillations in the solution in regions where there are strong gradients of the variable being solved.

Imposition of the boundedness property leads to the so-called high resolution schemes (HRS) [7, 8] which allow for good resolution of shocks or steep gradients without introducing oscillations in the solution. In the total-variation-diminishing approach for constructing HRS (TVD [7]), flux limiter functions were introduced to guarantee that values of a conserved property remain within the bounds imposed by neighbouring values; examples are the MINMOD limiter of Roe or Harten (e.g. Reference [7]) and the Van Leer harmonic limiter [9]. An important clarifying tool was later introduced by Gaskell and Lau [10] and Leonard [11] for steady flows, and extended to unsteady flows by Leonard [12] (see also the more recent overview, Reference [13]), under the form of the normalized variable diagram NVD and the convection boundedness criterion CBC. A number of previously proposed TVD flux limiters can be re-interpreted in the NVD, as shown by Leonard [12], allowing for an easier understanding of their characteristics. Of special interest here is the high resolution SMART scheme proposed by Gaskell and Lau [10] for steady-state implicit calculations, which is a limited (bounded) version of QUICK devised in the NVD, and will be the base for the present proposal.

Extension of HRS to non-uniform mesh spacing has led to the normalized variable and space formulation (NVSF [14]), which has been employed in References [15, 16] for the simulation of viscoelastic fluid flow. The problem with viscoelastic flow simulations lies on the representation of the advective terms in the differential transport-like equations for the stress tensor. Although the problem of excessive numerical diffusion could be solved with the HRSs, another problem resulted: iterative convergence was impaired when the equations were solved implicitly for a steady-state solution. Convergence difficulties with HRS have been experienced earlier; Gaskell and Lau [10] recommended the use of under-relaxation for the cell face fluxes obtained with their SMART scheme in order to dampen oscillatory iteration behaviour, and similar findings are reported by others [17–19]. Most of the HRS are constructed as composite functions in the NVD and switching instabilities may arise leading to lack of iterative convergence. For example, Zhu [17] and Jasak *et al.* [20] have developed their schemes either by using curved lines in the NVD or by devising smooth transitions between the patched lines representing each separate scheme. We found that a smooth characteristic of a given scheme in the NVD does not always guarantee iterative convergence and a second condition, related to TVD constraints, needs to be fulfilled.

The focus of the present paper is to devise an HRS, in the NVD, with better iterative convergence properties than the existing schemes, but with as good accuracy as the SMART scheme (i.e. formally third-order on uniform meshes). In order to accomplish this, we have incorporated into the formulation of the scheme the TVD constraints, which are known [13] to be required for explicit transient calculations. The proposed scheme is demonstrated with three problems: the classical accuracy tests of pure advection of a step, sine-square and semi-ellipse profiles at 30 and 45 degrees to a uniform mesh; the laminar Newtonian flow over a

two-dimensional backward-facing step; and a viscoelastic fluid flow through a planar contraction and around a cylinder.

2. GOVERNING EQUATIONS

In any incompressible fluid flow problem the basic equations to be solved are those expressing conservation of mass and linear momentum:

$$\frac{\partial u_j}{\partial x_j} = 0 \tag{1}$$

$$\frac{\partial \rho u_i}{\partial t} + \frac{\partial \rho u_j u_i}{\partial x_j} = -\frac{\partial p}{\partial x_i} + \frac{\partial \tau_{ij}}{\partial x_j} \tag{2}$$

where standard tensor notation with summation of repeated indices is employed, ρ is the fluid density and u_i the velocity component along the Cartesian co-ordinate x_i. The dependent variables are the velocity components, pressure p and the extra stress components τ_{ij}, which need to be specified by means of a rheological constitutive equation. In this work two types of constitutive equations are considered. The first is the Newtonian model expressed by a linear and explicit stress–strain rate relationship,

$$\tau_{ij} = \eta\left(\frac{\partial u_i}{\partial x_j} + \frac{\partial u_j}{\partial x_i}\right) \tag{3}$$

where η is the constant viscosity of the fluid. As a second type of constitutive equation we take one appropriate for modelling viscoelastic flow behaviour, known as the upper convected Maxwell (UCM) model [21], and expressed by the following differential transport-like equation for τ_{ij}:

$$\tau_{ij} + \lambda\left(\frac{\partial \tau_{ij}}{\partial t} + \frac{\partial u_k \tau_{ij}}{\partial x_k}\right) = \eta\left(\frac{\partial u_i}{\partial x_j} + \frac{\partial u_j}{\partial x_i}\right) + \lambda\left(\tau_{ik}\frac{\partial u_j}{\partial x_k} + \tau_{jk}\frac{\partial u_i}{\partial x_k}\right) \tag{4}$$

where λ is the relaxation time of the fluid. Although Equation (4) is one of the simplest models to represent viscoelastic fluid behaviour, it is also one of the most challenging from the numerical point of view [22] because it induces very high stresses near corners and other singular points in a flow configuration. Furthermore, due to its hyperbolic nature (notice the absence of any stress diffusion term in Equation (4)) this constitutive equation serves well our purpose as a suitable model for assessing the HRS here developed. In fact, it is known [22] that standard upwind schemes simply lead to exaggerated numerical diffusion and are not adequate for equations like Equation (4).

3. BASIC NUMERICAL METHODOLOGY

The finite-volume numerical method utilized in this work is only briefly outlined below as it has been previously described in some detail [23]. The focus here is on the description of the new high resolution scheme and an overview of the NVD and other HRSs is given first.

3.1. General discretization

A collocated variable arrangement is employed in which all variables ($\phi \equiv u_i, \tau_{ij}$) are stored at the centre of the control-volumes (cells) composing the computational mesh. Discretization of the momentum (Equation (2)) and constitutive equations (Equations (3) or (4)) over a general cell P leads to a linearized algebraic equation of the form:

$$a_P \phi_P = \sum_F^6 a_F \phi_F + S_\phi \tag{5}$$

where ϕ_P and ϕ_F represent the variable in cell P and neighbour cells F, a_F and a_P are coefficients, and S_ϕ is the source term. The time dependent terms in Equations (2) and (4) are discretized with the first-order backward Euler scheme and are included in a_P and S_ϕ where they act as inertial under-relaxation (see e.g. Reference [2]). The ϕ's in Equation (5) are assumed to pertain to a new time level and so Equation (5) is fully implicit in ϕ, thus requiring a linear-equation solver in order to update the ϕ field—we have used conjugate-gradient methods (see Reference [23]). All terms in the governing equations are discretized in space by means of central differences (CDS) and linear interpolation, except the advective terms which are discretized with the HRS and implemented through the deferred correction approach of Khosla and Rubin [24]. This implies that the coefficients a_F and a_P are based on UDS (thus ensuring positive coefficients) and the difference between the HRS fluxes and the UDS fluxes are evaluated at the previous time level and included in the source term.

The main advantages of deferred correction are stability, simplicity and computer-memory saving. The latter results from the fact that the same coefficients a_P and a_F are employed for the three velocity components, when solving the momentum equations, and for the six stress equations, when solving the constitutive equations. In general the deferred correction approach tends to promote numerical stability, as it ensures that the coefficient matrix is (more) diagonal dominant. The convergence rate, measured by the number of time steps required to attain a steady solution, may be worst than that achieved with a specific implementation of each HRS (cf. the curvature-factor method of Reference [10] for the SMART scheme; see also Reference [25]). This, however, would be too involved in terms of coding and, in any case, with deferred correction the iterative performance of each HRS is comparable on an equal basis. It is noted that the deferred correction may lead to unbounded fields during the time-marching advancement procedure, before the steady-state solution is reached. This issue is more important for pure advection, without physical sources, a situation somewhat removed from our main motivation (both the momentum and constitutive equations for viscoelastic flows have sources); but, again, it is fair to assume that all schemes will be equally affected by this problem.

3.2. Generalities on high resolution schemes and the NVD

We follow the NVD approach introduced by Gaskell and Lau [10] and Leonard [11, 12]. In this formulation the advected variable ϕ is normalized as

$$\widehat{\phi} = \frac{\phi - \phi_U}{\phi_D - \phi_U} \tag{6}$$

where the subscripts U and D refer to the upstream and downstream cells to cell P which is, itself, upstream of the cell face f under consideration, as shown in Figure 1. Note that

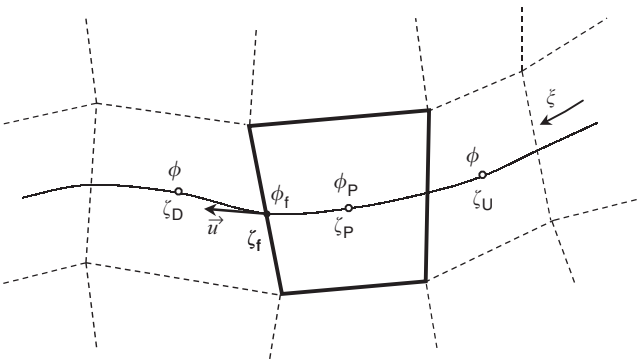

Figure 1. Definition of local variables and co-ordinate system.

this labelling of the nodes depends on the flux direction. In general, any differencing scheme (of third-order or less) that evaluates a cell face value ϕ_f as a function of the neighbour cell values (U, P and D) can be written under a simplified functional form, $\widehat{\phi}_f = f(\widehat{\phi}_P)$, where the normalization defined by Equation (6) is employed. For the general case of non-uniform meshes [14] the normalized cell face value of any variable becomes a function of both its closest normalized upwind neighbour value and the corresponding normalized locations, as

$$\widehat{\phi}_f = f(\widehat{\phi}_P, \widehat{\xi}_P, \widehat{\xi}_f) \tag{7}$$

where the normalized co-ordinates (see Figure 1) are:

$$\widehat{\xi}_P = \frac{\xi_P - \xi_U}{\xi_D - \xi_U} \quad \text{and} \quad \widehat{\xi}_f = \frac{\xi_f - \xi_U}{\xi_D - \xi_U} \tag{8}$$

Occurrence of unphysical oscillations in a solution for ϕ can be avoided if the cell face value ϕ_f lies within the bounds imposed by neighbouring nodal values, ϕ_P and ϕ_D, following the Convection Boundedness Criterion (CBC) of Gaskell and Lau [10], valid for implicit steady-state flow calculations. The CBC is illustrated in the NVD (see Figure 2) by the shadowed area together with the line with slope one outside that area. The various straight lines in Figure 2 represent the basic schemes: first-order upwind (UDS); second-order upwind (LUDS); third-order upwind (QUICK); second-order central (CDS). Clearly, UDS is the only basic differencing scheme that satisfies the CBC and only a non-linear function in the NVD can represent a bounded scheme of order higher than unity.

Once the required conditions for boundedness are known, construction of a high resolution scheme in the NVD is straightforward (see Reference [12]). Several composite schemes have been reported in the literature and some of the most popular of these non-linear schemes are plotted in Figure 3 and presented in Table I using either the NVD, valid for uniform meshes, or more generally the NVSF, valid for arbitrary non-uniform meshes. Various high-resolution schemes, known by the acronyms MINMOD [7], SMART [10] and WACEB [19], were constructed combining, in a piecewise way, straight lines in the NVD. Schemes composed by curved lines in the NVD have also been proposed, like the harmonic or CLAM ('curved-line advection method') scheme of van Leer [9] (also known as HPLA, proposed independently by

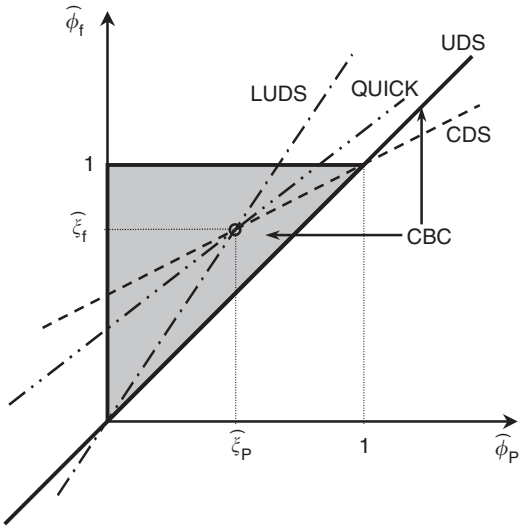

Figure 2. Normalized variable diagram (NVD) for different interpolation schemes showing the convective boundedness criterion (CBC). (Differencing schemes: UDS ≡ upwind, LUDS ≡ linear upwind, QUICK ≡ quadratic upwind, CDS ≡ central).

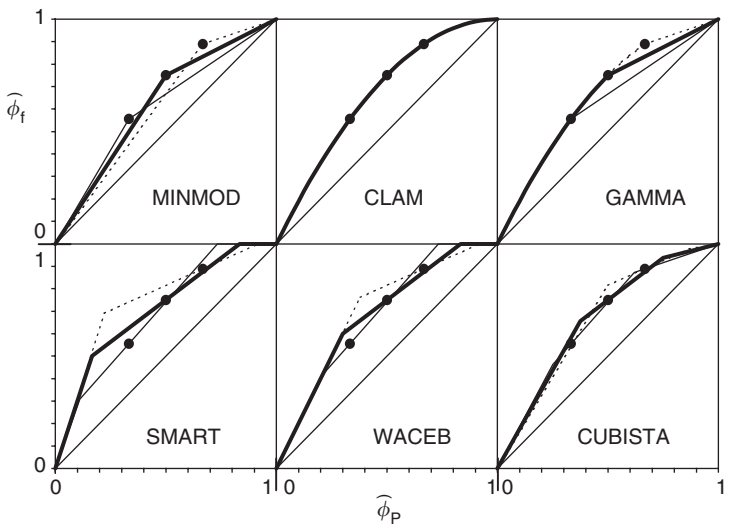

Figure 3. NVD plots of the high-resolution schemes used in this work for (——) uniform mesh, (——) non-uniform mesh with a constant expansion ratio of 2 and (- - - -) non-uniform mesh with a constant compression ratio of 0.5. The full circles represent the smooth flow point for each situation, and correspond to the co-ordinates $(\widehat{\xi}_P, \widehat{\xi}_f)$.

Zhu [17]) and the more recent GAMMA scheme of Jasak *et al.* [20]. The schemes in Table I are formally second-order accurate, with exception of the SMART and WACEB schemes which may achieve third-order accuracy on uniform meshes.

Table I. Functional relationship of some high-resolution schemes according to the NVD (uniform meshes) and the NVSF (non-uniform meshes).

	NVSF	NVD
MINMOD [7]	$\widehat{\phi}_f = \begin{cases} \frac{\widehat{\xi}_f}{\widehat{\xi}_P}\widehat{\phi}_P & 0 < \widehat{\phi}_P < \widehat{\xi}_P \\ \frac{1-\widehat{\xi}_f}{1-\widehat{\xi}_P}\widehat{\phi}_P + \frac{\widehat{\xi}_f - \widehat{\xi}_P}{1-\widehat{\xi}_P} & \widehat{\xi}_P \leqslant \widehat{\phi}_P < 1 \\ \widehat{\phi}_P & \text{elsewhere} \end{cases}$	$\widehat{\phi}_f = \begin{cases} \frac{3}{2}\widehat{\phi}_P & 0 < \widehat{\phi}_P < \frac{1}{2} \\ \frac{1}{2}\widehat{\phi}_P + \frac{1}{2} & \frac{1}{2} \leqslant \widehat{\phi}_P < 1 \\ \widehat{\phi}_P & \text{elsewhere} \end{cases}$
SMART [10]	$\widehat{\phi}_f = \begin{cases} \frac{\widehat{\xi}_f(1-3\widehat{\xi}_P+2\widehat{\xi}_f)}{\widehat{\xi}_P(1-\widehat{\xi}_P)}\widehat{\phi}_P & 0 < \widehat{\phi}_P < \frac{\widehat{\xi}_P}{3} \\ \frac{\widehat{\xi}_f(1-\widehat{\xi}_f)}{\widehat{\xi}_P(1-\widehat{\xi}_P)}\widehat{\phi}_P + \frac{\widehat{\xi}_f(\widehat{\xi}_f - \widehat{\xi}_P)}{1-\widehat{\xi}_P} & \frac{\widehat{\xi}_P}{3} \leqslant \widehat{\phi}_P \leqslant \frac{\widehat{\xi}_P}{\widehat{\xi}_f}(1+\widehat{\xi}_f - \widehat{\xi}_P) \\ 1 & \frac{\widehat{\xi}_P}{\widehat{\xi}_f}(1+\widehat{\xi}_f - \widehat{\xi}_P) < \widehat{\phi}_P < 1 \\ \widehat{\phi}_P & \text{elsewhere} \end{cases}$	$\widehat{\phi}_f = \begin{cases} 3\widehat{\phi}_P & 0 < \widehat{\phi}_P < \frac{1}{6} \\ \frac{3}{4}\widehat{\phi}_P + \frac{3}{8} & \frac{1}{6} \leqslant \widehat{\phi}_P \leqslant \frac{5}{6} \\ 1 & \frac{5}{6} < \widehat{\phi}_P < 1 \\ \widehat{\phi}_P & \text{elsewhere} \end{cases}$
CLAM [9]	$\widehat{\phi}_f = \begin{cases} \frac{\widehat{\xi}_f - \widehat{\xi}_P^2}{\widehat{\xi}_P(1-\widehat{\xi}_P)}\widehat{\phi}_P - \frac{\widehat{\xi}_f - \widehat{\xi}_P}{\widehat{\xi}_P(1-\widehat{\xi}_P)}\widehat{\phi}_P^2 & 0 < \widehat{\phi}_P < 1 \\ \widehat{\phi}_P & \text{elsewhere} \end{cases}$	$\widehat{\phi}_f = \begin{cases} \widehat{\phi}_P(2-\widehat{\phi}_P) & 0 < \widehat{\phi}_P < 1 \\ \widehat{\phi}_P & \text{elsewhere} \end{cases}$

Table I. (*Continued*).

	NVSF	NVD
WACEB [19]	$\widehat{\phi}_f = \begin{cases} 2\widehat{\phi}_P & 0 < \widehat{\phi}_P < \dfrac{\widehat{\xi}_P \widehat{\xi}_f (\widehat{\xi}_f - \widehat{\xi}_P)}{2\,\widehat{\xi}_P(1-\widehat{\xi}_P) - \widehat{\xi}_f(1-\widehat{\xi}_f)} \\ \dfrac{\widehat{\xi}_f(1-\widehat{\xi}_f)}{\widehat{\xi}_P(1-\widehat{\xi}_P)}\widehat{\phi}_P + \dfrac{\widehat{\xi}_f(\widehat{\xi}_f - \widehat{\xi}_P)}{1-\widehat{\xi}_P} & \dfrac{\widehat{\xi}_P \widehat{\xi}_f (\widehat{\xi}_f - \widehat{\xi}_P)}{2\,\widehat{\xi}_P(1-\widehat{\xi}_P) - \widehat{\xi}_f(1-\widehat{\xi}_f)} \leqslant \widehat{\phi}_P \leqslant \dfrac{\widehat{\xi}_P}{\widehat{\xi}_f}(1+\widehat{\xi}_f - \widehat{\xi}_P) \\ 1 & \dfrac{\widehat{\xi}_P}{\widehat{\xi}_f}(1+\widehat{\xi}_f - \widehat{\xi}_P) < \widehat{\phi}_P < 1 \\ \widehat{\phi}_P & \text{elsewhere} \end{cases}$	$\widehat{\phi}_f = \begin{cases} 2\widehat{\phi}_P & 0 < \widehat{\phi}_P < \frac{3}{10} \\ \frac{3}{4}\widehat{\phi}_P + \frac{3}{8} & \frac{3}{10} \leqslant \widehat{\phi}_P \leqslant \frac{5}{6} \\ 1 & \frac{5}{6} < \widehat{\phi}_P < 1 \\ \widehat{\phi}_P & \text{elsewhere} \end{cases}$
GAMMA [20]*	$\widehat{\phi}_f = \begin{cases} \widehat{\phi}_P \left[1 + \dfrac{1}{\beta_m}\dfrac{\widehat{\xi}_f - \widehat{\xi}_P}{1-\widehat{\xi}_P}(1-\widehat{\phi}_P)\right] & 0 < \widehat{\phi}_P < \beta_m \\ \dfrac{1-\widehat{\xi}_f}{1-\widehat{\xi}_P}\widehat{\phi}_P + \dfrac{\widehat{\xi}_f - \widehat{\xi}_P}{1-\widehat{\xi}_P} & \beta_m \leqslant \widehat{\phi}_P < 1 \\ \widehat{\phi}_P & \text{elsewhere} \end{cases}$	$\widehat{\phi}_f = \begin{cases} \widehat{\phi}_P \left[1 + \dfrac{1}{2\beta_m}(1-\widehat{\phi}_P)\right] & 0 < \widehat{\phi}_P < \beta_m \\ \frac{1}{2}\widehat{\phi}_P + \frac{1}{2} & \beta_m \leqslant \widehat{\phi}_P < 1 \\ \widehat{\phi}_P & \text{elsewhere} \end{cases}$

*NVD from original paper; NVSF here derived.

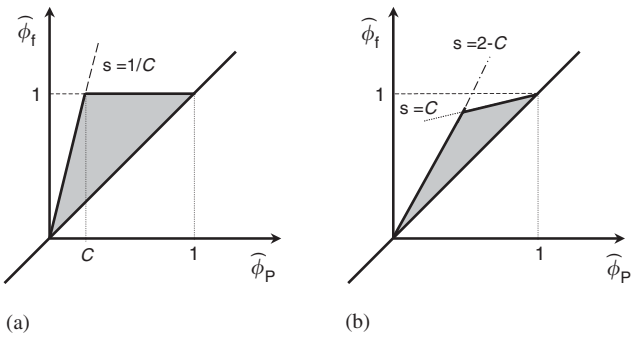

Figure 4. (a) Universal limiter and; (b) TVD constraints for explicit unsteady calculations.

4. PROPOSED HRS

As alluded to in the Introduction, an important issue arising in relation to all those composite HRS is linked to their convergence properties. We are not as much concerned with accuracy, since second or even third-order accuracy in truncation error can easily be accomplished by increasing the complexity of the interpolation of the basic scheme, but with the important point of ensuring that the algebraic equations resulting from the implicit discretization can be converged to a prescribed tolerance. It is known [10, 17–20] that due to their composite nature, these HRS are prone to numerical instabilities, for example whenever a given nodal value is in such a situation that the schemes jump from one of the composing schemes to another. One aspect, that is often overseen and which is the main motivation for the present study, is that the CBC by itself does not guarantee a bounded scheme to always produce a converged solution. Less general conditions than the CBC are required to guarantee convergence of iterative schemes.

Leonard [12] has introduced the notion of the Universal Limiter (ULTIMATE) valid for explicit transient calculations (Figure 4(a)), which reduces to the CBC for steady flows when the Courant number tends to zero, $C \to 0$. For small values of C, the ULTIMATE differs from the CBC in the region of positive values of $\widehat{\phi}_P$ close to the origin, as seen in Figure 4(a), where a Courant number condition must be observed

$$\widehat{\phi}_P \leqslant \widehat{\phi}_f \leqslant \frac{1}{C}\,\widehat{\phi}_P \quad \text{for } 0 \leqslant \widehat{\phi}_P \leqslant C \tag{9}$$

On the other hand, the conditions for an explicit time-dependent method to be TVD [8], namely:

$$\begin{aligned} &\widehat{\phi}_P \leqslant \widehat{\phi}_f \leqslant (2-C)\widehat{\phi}_P \qquad (\text{left-side of NVD, } \widehat{\phi}_P \leqslant \tfrac{1}{2}) \\ &\widehat{\phi}_P \leqslant \widehat{\phi}_f \leqslant 1 - C(1-\widehat{\phi}_P) \quad (\text{right-side of NVD, } \widehat{\phi}_P \geqslant \tfrac{1}{2}) \end{aligned} \tag{10}$$

are even more restrictive than the universal limiter of Leonard, and the allowable area on a $\widehat{\phi}_f$ versus $\widehat{\phi}_P$ plot is further reduced, as shown in Figure 4(b) (see also Reference [13, p. 45]). This is not surprising because, mathematically, the TVD condition is more severe than the

boundedness condition (or monotonicity-preserving condition, on which the ULTIMATE and the CBC are based), but it is sufficient to guarantee the convergence of the numerical solution of a conservative scheme to the weak solution of the underlying conservation law [26, pp. 525–529]. And even if the TVD conditions are still not sufficient to assure satisfaction of the entropy condition, experience has shown that TVD schemes tend to converge to physically acceptable solutions [8].

In essential terms, the main contribution of the present paper is to recognise the importance of satisfying the TVD constraints of Figure 4(b), that is Equations (10) together with the CBC, and their connection with iterative convergence properties. A new HRS embodying those notions was then devised, combining accuracy with better iterative convergence properties, and its construction and the rationale behind it are described in the following points, in connection to the NVD for uniform meshes (for convenience):

(i) *The basic scheme and accuracy*: The basic differencing scheme should be as accurate as possible and so the formally third-order accurate QUICK scheme is selected for that role. Leonard [12, 13] has amply demonstrated that in all his test cases QUICK gives better resolution than second-order upwind, central differencing or Fromm's differencing (a mixture of LUDS and CDS). Furthermore, when the NVD approach is followed, the implementation of QUICK does not add any significant complexity compared to the implementation of those second-order schemes.

(ii) *The smooth region*: Changes of slope of the scheme representation in the NVD should be avoided in the smooth flow region (i.e. $0.4 \leqslant \widehat{\phi}_P \leqslant 0.6$). Numerical experiments have shown that when a scheme has an abrupt change of slope at $\widehat{\phi}_P = 0.5$, it tends to exhibit problems of iterative convergence (see the Results section for the MINMOD scheme). As a consequence, the line $\frac{3}{8} + \frac{3}{4}\widehat{\phi}_P$ representing the basic QUICK differencing scheme should be prolonged, as far as possible, to the left and right of $\widehat{\phi}_P = 0.5$.

(iii) *The TVD constraints*: The scheme should respect the TVD restrictions of Equations (10) and Figure 4(b), with C taken as an empirical parameter to be found by numerical experiments. If the less restrictive CBC (or ULTIMATE, with $C = 0$) condition were adopted, then we would end up with the SMART scheme, composed by the QUICK straight line $\frac{3}{8} + \frac{3}{4}\widehat{\phi}_P$, a portion of the downwind line (constant $\widehat{\phi}_f = 1$) close to $\widehat{\phi}_P = 1$, and a straight line with slope 3 connecting to $\widehat{\phi}_P = 0$. Similarly, for the TVD conditions valid for steady state ($C = 0$), we would end up with the WACEB scheme [19], whereby the only difference with SMART is the line of slope 2, instead of 3, connecting the QUICK line to the origin.

(iv) *The choice of parameter C*: Our interest is in steady-state solutions but since these are reached by an implicit time-marching approach there will be 'some' similarity with truly time-dependent calculations. The TVD constraints of Figure 4(b) were derived from explicit time-advancement procedures which have to respect the CFL requirement ($C \leqslant 1$). We can also define a local Courant number (e.g. $C = \mathrm{Max}(u\delta t/\delta x, v\delta t/\delta y)$) but it will be much higher than unity (of order ≈ 10) due to the fully-implicit nature of the algorithm and the fact that we are not interested in resolving the time evolution accurately. We cannot therefore take C in the TVD as a true Courant number, but rather as a parameter. If $C = 0$, our scheme reduces to the recently proposed WACEB scheme; however, as will be seen in the Results section, this scheme still has convergence problems for some flow problems. Numerical experiments showed that by increasing C to 0.1, iterative convergence could be attained for some cases, but

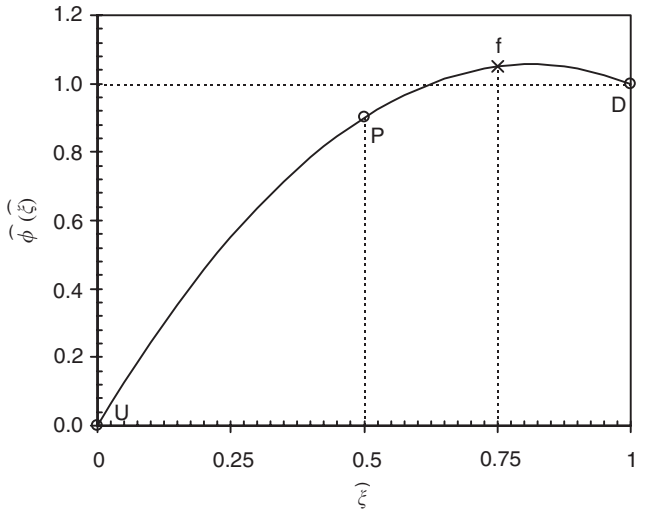

Figure 5. Sketch of a situation leading to interpolation overshoot with QUICK ($\widehat{\phi}_P = 0.9$).

would persist in the viscoelastic flow case. A value of $C = 0.25$ was found to give converged results in all cases tested (not all are reported here). Of course C should be kept as low as possible in order to avoid too much dissipation in the flow regions where $\widehat{\phi}_P \approx 0$ or $\widehat{\phi}_P \approx 1$. There is, therefore, a compromise between increasing C (restricting the allowable NVD area) in order to promote convergence, and decreasing C to improve resolution of sharp gradients. The value $C = 0.25$ seems to be optimal in this respect.

(v) *The problematic downwind line*: Although the value of $C = 0.25$ was initially selected based on numerical experiments, as explained in the previous point, there is a more formal argument for that choice. The most problematic region of all the HRS's mentioned beforehand is the downwind line close to the upper limit of the monotone range in the NVD ($\widehat{\phi}_P \to 1$). Pure downwind yields a single negative coefficient in the discretized equations and that is always troublesome for implicit solution methods (a specific treatment is required, e.g. Reference [25]). Now, when $\widehat{\phi}_P$ increases from values typical of the smooth region, at a certain stage the parabolic interpolation line representing the QUICK scheme (ξ is a local coordinate: $\phi_P = \phi(0)$; $\phi_D = \phi(1)$; $\phi_U = \phi(-1)$):

$$\phi(\xi) = \phi_P + \frac{\phi_D - \phi_U}{2}\,\xi + \frac{\phi_D + \phi_U - 2\phi_P}{2}\,\xi^2 \tag{11}$$

reaches the situation sketched in Figure 5. There is an overshoot of $\widehat{\phi}$ and monotonicity is not preserved; it is then that downwind is called for, and the problems mentioned above start. The precise point leading to the overshoot situation can be determined from the condition:

$$\left[\frac{\partial \phi}{\partial \xi}\right]_{\xi \to 1} \leqslant 0 \;\Rightarrow\; \frac{3\phi_D + \phi_U - 4\phi_P}{2} \leqslant 0$$

giving:

$$\widehat{\phi}_P \equiv \frac{\phi_P - \phi_U}{\phi_D - \phi_U} \geqslant \frac{3}{4} \tag{12}$$

So for values of $\widehat{\phi}_P$ higher than 0.75 (corresponding to $(\widehat{\phi}_f)_{QUICK} = 0.9375$) it is unsafe to pursue along the QUICK line, as that gives rise to interpolation overshoot, instead one should safely follow the line connecting the point (0.75, 0.9375) to (1,1) in the NVD. That gives a slope $C = 0.25$, the same value obtained from the numerical experiments.

(vi) *Symmetry conditions for the limiter*: From the previous considerations, the proposed scheme will have a piecewise linear representation in the monotonic range of the NVD ($0 \leqslant \widehat{\phi}_P \leqslant 1$) composed by three segments: TVD limiter on the left ($\widehat{\phi}_P \approx 0$), i.e. straight line with slope $2 - C$ passing through the origin; QUICK line ($\frac{3}{8} + \frac{3}{4}\widehat{\phi}_P$) on the middle region corresponding to the smooth flow regime; and TVD limiter on the right ($\widehat{\phi}_P \approx 1$), i.e. straight line with slope $+C$ passing through the point $\widehat{\phi}_P = 1$, $\widehat{\phi}_f = 1$. Since C is a free parameter, and not a real Courant number, we could have chosen different values of C for the left slope $2 - C$ (say C_1) and the right slope $+C$ (say C_2) of the TVD limiter. This would, however, violate the condition for a symmetric limiter [8] with the consequence that given symmetric profiles would tend to be distorted when advected. This is readily seen by translating the proposed scheme from the NVD to Sweby's diagram [8] ($\varphi(r)$ versus r) giving:

$$\varphi(r) = \text{Max}\left\{0, \text{Min}\left[2r(1 - C_1), \frac{3}{4} + \frac{r}{4}, 2(1 - C_2)\right]\right\} \tag{13}$$

where φ is the flux limiter factor of Sweby, and r the ratio of consecutive gradients ($\varphi = (\widehat{\phi}_f - \widehat{\phi}_P)/0.5(1 - \widehat{\phi}_P)$ and $r \equiv (\phi_P - \phi_U)/(\phi_D - \phi_P) = \widehat{\phi}_P/(1 - \widehat{\phi}_P)$; see also Appendix B in Reference [12]). The condition for a symmetric limiter is

$$\frac{\varphi(r)}{r} = \varphi\left(\frac{1}{r}\right) \tag{14}$$

giving:

$$\begin{aligned}\varphi\left(\frac{1}{r}\right) &= \text{Max}\left\{0, \text{Min}\left[2\frac{1}{r}(1 - C_1), \frac{3}{4} + \frac{1}{4r}, 2(1 - C_2)\right]\right\} \\ &= \frac{1}{r}\,\text{Max}\left\{0, \text{Min}\left[2(1 - C_1), \frac{3}{4}r + \frac{1}{4}, 2(1 - C_2)r\right]\right\}\end{aligned} \tag{15}$$

for our scheme. Comparing (15) with the previous expression for $\varphi(r)$, Equation (13), we see that (approximate) symmetry is achieved provided the same C ($C_1 = C_2$) is used at both extremities of the limiter function (approximate because the middle QUICK line cannot, of course, be strictly symmetric—this does not affect the symmetry of advected profiles). For this reason the same $C = 0.25$ is adopted for both TVD slopes.

The NVD description of the proposed scheme, coined CUBISTA (for Convergent and Universally Bounded Interpolation Scheme for Treatment of Advection), is therefore given by

$$\widehat{\phi}_{\mathrm{f}} = \begin{cases} \frac{7}{4}\widehat{\phi}_{\mathrm{P}} & 0 < \widehat{\phi}_{\mathrm{P}} < \frac{3}{8} \\ \frac{3}{4}\widehat{\phi}_{\mathrm{P}} + \frac{3}{8} & \frac{3}{8} \leqslant \widehat{\phi}_{\mathrm{P}} \leqslant \frac{3}{4} \\ \frac{1}{4}\widehat{\phi}_{\mathrm{P}} + \frac{3}{4} & \frac{3}{4} < \widehat{\phi}_{\mathrm{P}} < 1 \\ \widehat{\phi}_{\mathrm{P}} & \text{elsewhere} \end{cases} \tag{16}$$

It is an easy matter to transform these relations for the case of non-uniform meshes, by following the NVSF formulation of Reference [14]; the result is

$$\widehat{\phi}_{\mathrm{f}} = \begin{cases} \left[1 + \dfrac{\widehat{\xi}_{\mathrm{f}} - \widehat{\xi}_{\mathrm{P}}}{3(1-\widehat{\xi}_{\mathrm{P}})}\right] \dfrac{\widehat{\xi}_{\mathrm{f}}}{\widehat{\xi}_{\mathrm{P}}}\,\widehat{\phi}_{\mathrm{P}} & 0 < \widehat{\phi}_{\mathrm{P}} < \dfrac{3}{4}\,\widehat{\xi}_{\mathrm{P}} \\ \dfrac{\widehat{\xi}_{\mathrm{f}}\,(1-\widehat{\xi}_{\mathrm{f}})}{\widehat{\xi}_{\mathrm{P}}\,(1-\widehat{\xi}_{\mathrm{P}})}\widehat{\phi}_{\mathrm{P}} + \dfrac{\widehat{\xi}_{\mathrm{f}}\,(\widehat{\xi}_{\mathrm{f}} - \widehat{\xi}_{\mathrm{P}})}{1-\widehat{\xi}_{\mathrm{P}}} & \dfrac{3}{4}\,\widehat{\xi}_{\mathrm{P}} \leqslant \widehat{\phi}_{\mathrm{P}} \leqslant \dfrac{1 + 2(\widehat{\xi}_{\mathrm{f}} - \widehat{\xi}_{\mathrm{P}})}{2\,\widehat{\xi}_{\mathrm{f}} - \widehat{\xi}_{\mathrm{P}}}\,\widehat{\xi}_{\mathrm{P}} \\ 1 - \dfrac{1-\widehat{\xi}_{\mathrm{f}}}{2(1-\widehat{\xi}_{\mathrm{P}})}(1-\widehat{\phi}_{\mathrm{P}}) & \dfrac{1 + 2(\widehat{\xi}_{\mathrm{f}} - \widehat{\xi}_{\mathrm{P}})}{2\,\widehat{\xi}_{\mathrm{f}} - \widehat{\xi}_{\mathrm{P}}}\,\widehat{\xi}_{\mathrm{P}} < \widehat{\phi}_{\mathrm{P}} < 1 \\ \widehat{\phi}_{\mathrm{P}} & \text{elsewhere} \end{cases} \tag{17}$$

The expressions are now more involved than (16), although still retaining the piecewise linear characteristics in the NVD, but are easy to code and implement in a systematic way. Note that the $\widehat{\xi}_{\mathrm{P}}, \widehat{\xi}_{\mathrm{f}}$ are geometric quantities, which are calculated once for each cell in the computational grid. The NVD plots of CUBISTA and the various other schemes used in this work are shown in Figure 3 for uniform (NVD) and non-uniform (NVSF) meshes.

5. RESULTS FROM APPLICATION TO TYPICAL PROBLEMS

The new high resolution CUBISTA scheme just described was implemented in a computer code and applied to three classes of problems. First, the classical test of pure advection of a scalar quantity by a skewed velocity field is considered, with view to assess the accuracy of the schemes. Then, two more complex flow situations were considered, exhibiting simultaneously advection–diffusion effects and recirculating regions, which are solved for both Newtonian and viscoelastic fluids: backward-facing step, planar contraction with a 4:1 ratio and flow around circular cylinder. The purpose here was to assess the iterative convergence properties of the high-resolution schemes presented in Table I, including the new scheme CUBISTA.

5.1. Pure advection of a passive scalar

In this first problem we consider the advective transport of a passive scalar by a given uniform velocity field, oblique to the mesh (at an angle θ). Under a two-dimensional situation, in a

square domain mapped with a Cartesian x, y mesh, the only conservation equation to be solved is

$$\frac{\partial(u\phi)}{\partial x} + \frac{\partial(v\phi)}{\partial y} = 0 \tag{18}$$

where ϕ is the advected variable and u and v are the Cartesian components of the given velocity vector. These are taken as either $u = v = \sqrt{2}/2$, which corresponds to a mesh-to-flow angle of 45°, or $u = \sqrt{3}/2,\ v = 0.5$ for an angle of 30°.

Three inlet boundary conditions have been used in these test cases corresponding to different profile shapes (for simplicity, here defined for $\theta = 45°$):

- Step profile

$$\begin{aligned} \phi(0, y) &= 1 \quad \text{for } 0 \leqslant y \leqslant 1 \\ \phi(x, 0) &= 0 \quad \text{for } 0 < x \leqslant 1 \end{aligned} \tag{19}$$

- Sine-square profile

$$\begin{aligned} \phi(0, y) &= \begin{cases} \sin^2(\frac{10}{3}\pi y) & \text{for } 0 \leqslant y \leqslant \frac{3}{20} \\ 1 & \text{for } \frac{3}{20} < y \leqslant 1 \end{cases} \\ \phi(x, 0) &= 0 \quad \text{for } 0 < x \leqslant 1 \end{aligned} \tag{20}$$

- Semi-ellipse profile (with a semi-width of 1/6)

$$\begin{aligned} \phi(0, y) &= \sqrt{1 - [(y/(1/6)]^2} \quad \text{for } |y| < 1/6 \\ \phi(0, y) &= 0 \quad \text{elsewhere} \end{aligned}$$

and

$$\begin{aligned} \phi(x, 0) &= \sqrt{1 - [x/(1/6)]^2} \quad \text{for } |x| < 1/6 \\ \phi(x, 0) &= 0 \quad \text{elsewhere} \end{aligned} \tag{21}$$

Each of these profile shapes serves a certain purpose in terms of scheme assessment: the step profile provides the stringent gradient variation, enabling assessment of the scheme's ability to resolve a sharp front, with minimum numerical diffusion and without oscillations. The sine-square is a relatively smooth profile enabling an assessment of the scheme's apparent order of accuracy. The semi-ellipse, due to the combination of opposed gradient discontinuities at the base with a region of slowly varying curvature without a sharp maximum, enables assessment of the steepening/clipping characteristics of the scheme, and its lack of symmetry. See also the discussion in Reference [12].

The resulting profiles of ϕ along the line $x = 0.5$ obtained on a uniform mesh consisting of 59×59 cells are given in Figures 6–8, for the three profile shapes, respectively, and for the two angles and the various discretization schemes. Note the enlarged scale for the abscissas in these figures, to better show differences amongst the schemes. As expected, the third-order

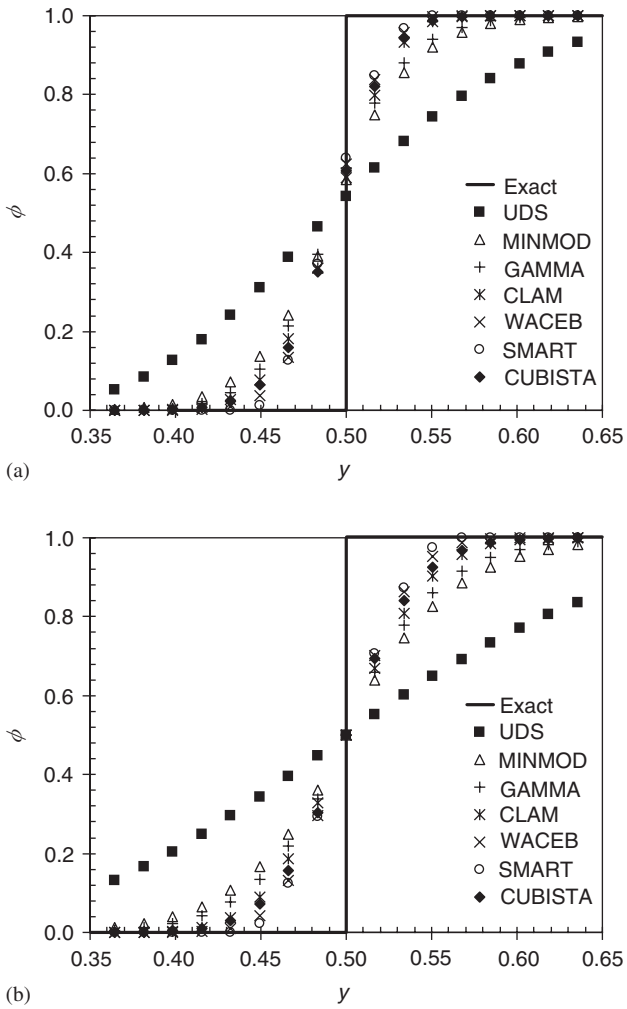

Figure 6. Results for the step profile along the line $x = 0.5$ on mesh 59×59: (a) angle of 30°; (b) angle of 45°.

SMART scheme is the least diffusive of the tested schemes for these linear problems, with the proposed CUBISTA scheme closely following the same results, while the UPWIND scheme clearly shows unacceptable levels of numerical diffusion. These figures also show that in general numerical diffusion is more accentuated for the angle 45° and the MINMOD results are still too diffusive.

Convergence with mesh refinement was studied for the case of the imposed sine-square profile, Equation (20). Figure 9 shows the absolute error, defined by the mean absolute difference between predicted and theoretical profiles along the line $x = 0.5$, for each differencing scheme and for different levels of refinement (four computational meshes). The apparent order of convergence of the differencing schemes is given by the slope of the lines shown in

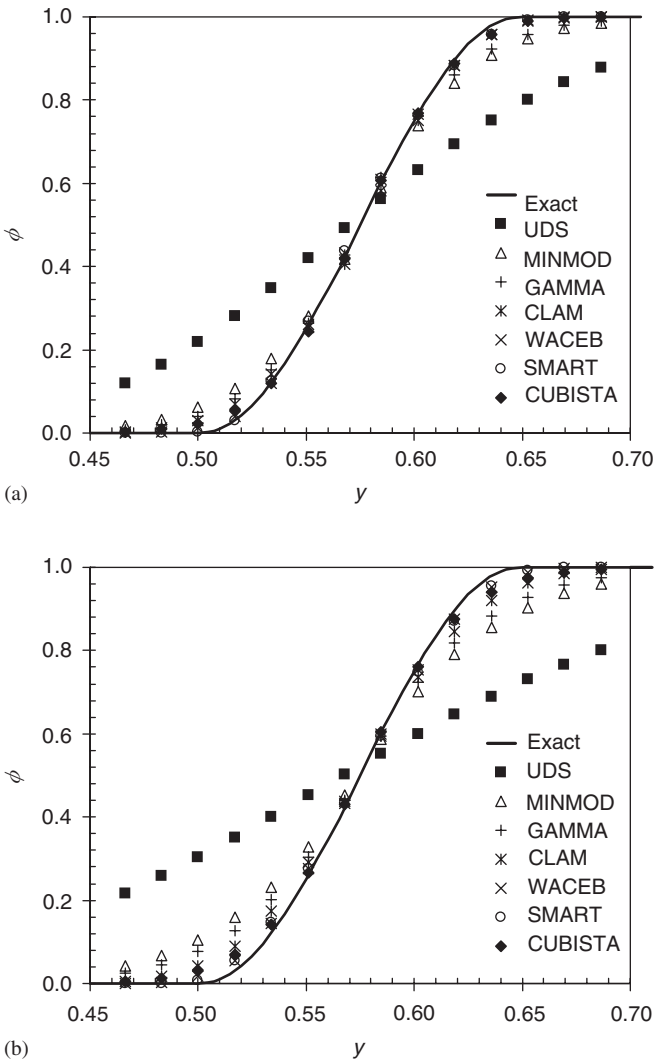

Figure 7. Results for the sine-square profile along the line $x = 0.5$ on mesh 59×59: (a) angle of 30°; (b) angle of 45°.

Figure 9. For the SMART scheme one obtains the theoretical third-order accuracy, while the CUBISTA and WACEB schemes exhibit somewhat smaller order of accuracy (2.7 and 2.6, respectively). This reduction in the order of accuracy results from the contribution of the two first points at the extremities of the profile which have, respectively, a $\widehat{\phi}_P$ smaller than 0.375 and larger than 0.75, and so give a face value which deviates from the third-order QUICK line. Strictly speaking, one should not evaluate the order of accuracy of a scheme in regions away from the smooth flow region (cf. Reference [11]). The CLAM, GAMMA and MINMOD schemes are approximately second-order accurate, as expected (the observed order is

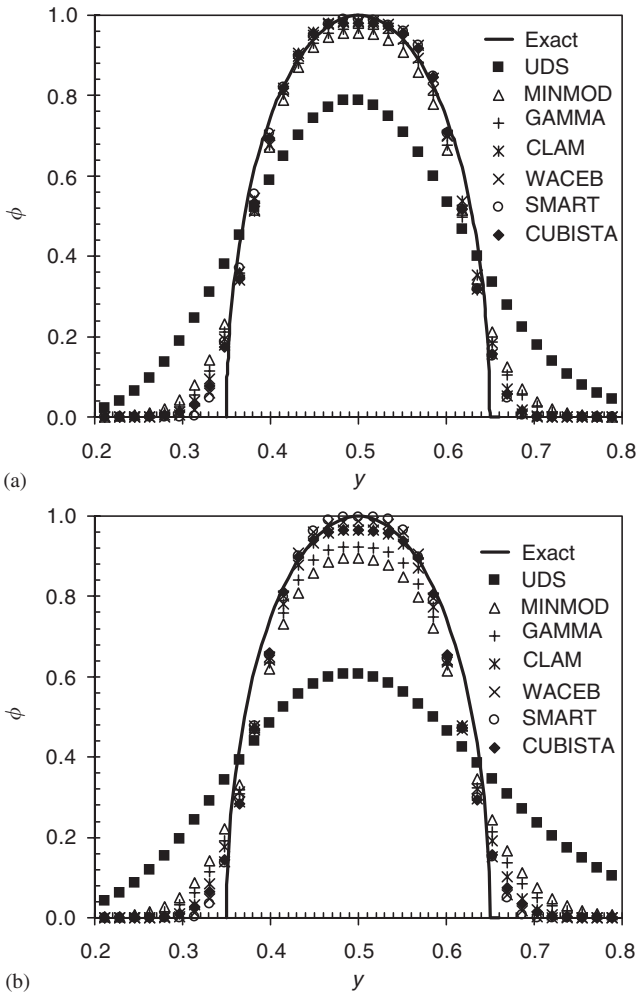

Figure 8. Results for the semi-ellipse profile along the line $x = 0.5$ on mesh 59×59: (a) angle of 30°; (b) angle of 45°.

somewhat less than the theoretical by the same reasons given above), but note that the absolute errors achieved with CLAM are significantly smaller than with the two other schemes. The upwind scheme is only first-order accurate, therefore leading to results which are generally too inaccurate.

To demonstrate the effects that asymmetry in the design of the schemes may have on the results, we show in Figure 10 several predictions for the semi-ellipse profile at an angle of 30°, with a coarser mesh (29×29). Both the SMART scheme and the GAMMA scheme with a smaller scheme parameter ($\beta_m = 0.1$, instead of 0.5 as before), used to improve resolution, show signs of asymmetrical resolution of the ellipse, due to a steepening/clipping effect discussed by Leonard [12]—the schemes are too compressive and transform smooth profiles into

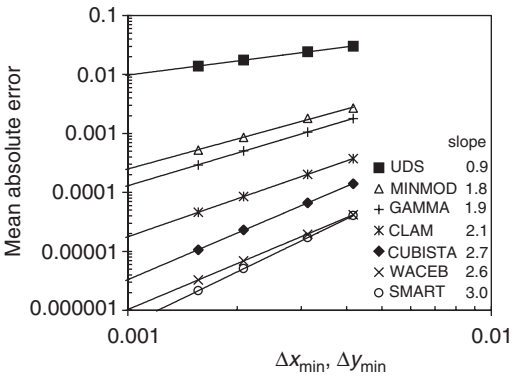

Figure 9. Mean absolute error between theoretical and computed profiles, versus the minimum grid spacing, for the sine-square case. The results presented were calculated for the profiles obtained along the line $x = 0.5$.

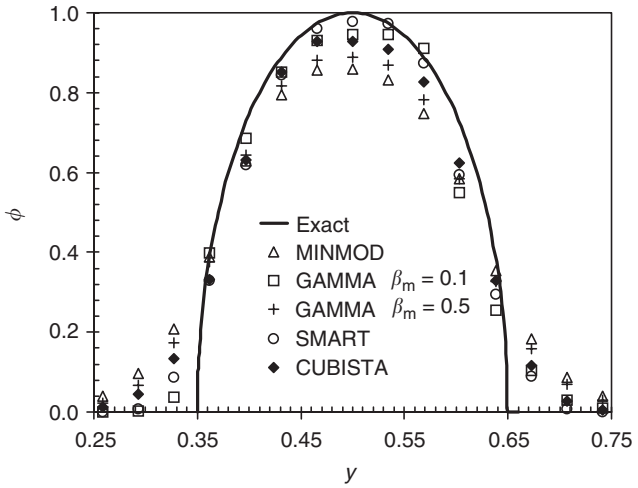

Figure 10. Effect of scheme's asymmetry: results for the semi-ellipse on mesh 29×29 at an angle of 30°.

sharp ones. The CUBISTA does not show that kind of behaviour and the ellipse is resolved symmetrically.

5.2. Laminar flow over a backward-facing step

The geometry of the plane backward-facing step is illustrated in Figure 11. This problem has been extensively studied, both experimentally and numerically, to the point that it became a typical benchmark problem for the numerical simulation of laminar flows e.g. References [27, 28]. The flow is characterized by two dimensionless parameters, the relative channel step height, s/h, and the Reynolds number, defined as $Re = 2\rho U_{in} h/\eta$, where U_{in} is the average

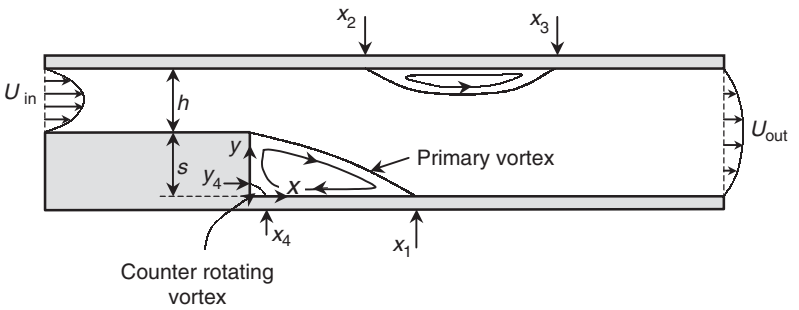

Figure 11. Sketch of the laminar backward-facing step geometry.

inlet velocity and h is the inlet channel height. In the present study we restrict our calculations to $s/h = 1$ and $Re = 800$. Two types of inlet conditions were used in accordance with previous numerical studies:

(i) Poiseuille flow imposed far from the step ($x/h = -20$)
(ii) Poiseuille flow imposed right at the step ($x/h = 0$).

Inlet type (ii) leads to longer main recirculating regions x_1 but otherwise the resulting flow fields are not significantly different. The outlet boundary is located at $x/h = 80$, which is sufficient for complete flow redevelopment with a Poiseuille profile at the exit. Preliminary simulations with shorter and longer downstream channels served to check that the results were not affected by that choice. The calculations were performed on several consecutively refined meshes in order to obtain very accurate grid-independent results, and also with view to evaluate the order of accuracy with mesh refinement of the various differencing schemes. We deal first with convergence issues and then with accuracy issues.

Since the main purpose of our scheme is to achieve good accuracy without deterioration in robustness, we compare in Figure 12 the evolution of the residuals of the u-momentum equation as a function of dimensionless time, $T = t/(2h/U_{in})$, for the various differencing schemes. This figure essentially shows the iterative convergence behaviour of the schemes, because the simulation time in the x-axis is proportional to the number of time steps. The residuals are defined as the L_1-norm of the algebraic equations to be solved and should tend to zero as the steady-state solution is approached. A converged solution was assumed when the normalized residuals of all equations fall below 10^{-5} and all cases in Figure 12 have been computed with a time step of $\delta T = 0.25$. Inspection of Figure 12 shows that the CLAM, WACEB and the proposed CUBISTA schemes converge at the same rate, but the SMART scheme is unable to converge to the prescribed tolerance. For the GAMMA scheme we used a parameter of $\beta_m = 0.5$ (to enhance stability) and the iterative behaviour is similar to that of the MINMOD, in line with the similarity between the NVD diagrams of these schemes.

We investigate next the effect of the time step on the convergence history for the problematic scheme, SMART. These results are presented in Figure 13 which shows the decay of residuals for a time step varying from 0.05 to 0.5, and the corresponding prediction of the extension of the main recirculation zone (cf. Figure 11). A fully converged solution with the SMART scheme requires smaller time increments, compared with the other schemes in Figure 12, and

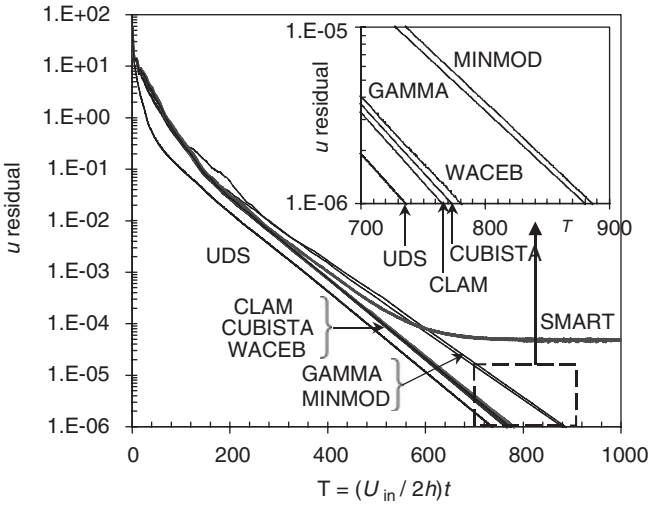

Figure 12. Decay of the norm of the residuals of the u momentum equation for the various differencing schemes, $\delta T = 0.25$.

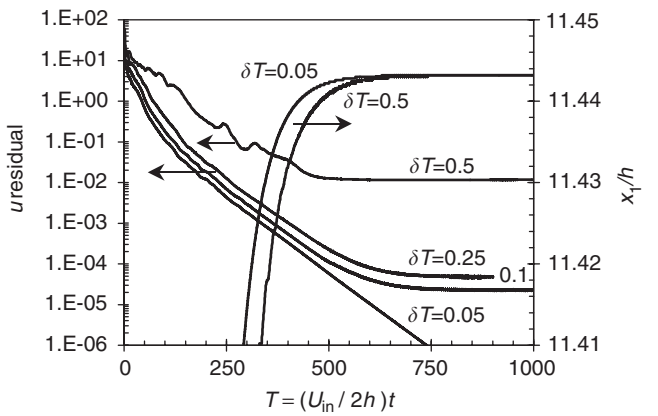

Figure 13. Decay of the norm of the residuals of the u-momentum equation for the SMART scheme. Influence of the time step on the convergence history.

consequently its convergence rate is reduced (by a factor of 5, in relation to CUBISTA). Figure 13 also shows, by looking simultaneously to the evolution of the residuals and of the predicted recirculation length x_1 for a time step of $\delta T = 0.5$, that the solution field is still varying when the residuals have already attained a certain stabilized lower level. It is true that in this case, by pursuing the calculations for more time steps, a unique solution (represented in Figure 13 by the same steady-state value of x_1) is eventually achieved. In general, however, it is not possible to ascertain whether lack of iterative convergence, indicated by a levelling out in the decay of the residuals, will eventually lead to an adequate non-varying solution

Table II. Primary-vortex dimension ($x_1/2h$) under steady-state conditions (with inlet channel).

Mesh*	$\Delta x_{\min}/2h$†	UDS	MINMOD	GAMMA	CLAM	WACEB	SMART	CUBISTA
51×20	0.0500				4.1380		4.3516	4.1042
102×40	0.0250	4.2156	5.3894	5.5546	5.6220	5.7188	5.7216	5.7125
153×60	0.0167	4.3532	5.7400	5.7894	5.7998	5.8351	5.8356	5.8338
204×80	0.0125	4.5948	5.8205	5.8457	5.8514	5.8701	5.8704	5.8697
306×120	0.00833	4.9665	5.8723	5.8835	5.8861	5.8938	5.8938	5.8936
408×160	0.00625	5.1968	5.8892	5.8955	5.8970	5.9012	5.9012	5.9012
	$x_{1,\mathrm{ref}}/2h$			5.9086	5.9086	5.9092	5.9092	5.9092
	n	1.0	2.1	2.2	2.2	2.3	2.3	2.3

*Without the portion for the inlet channel.
†$\Delta x_{\min} = \Delta y_{\min}$.

field. In the interest of robustness it is desirable to have a scheme which yields a decaying variation of residuals, whenever the time step is sufficiently small. Clearly, without further checks, it was not possible to decide whether the results with the SMART scheme and a δT of 0.1, 0.25 or 0.5 did correspond to the actual steady-state solution.

In Table II the predicted primary-vortex dimension under steady-state conditions (x_1) is presented for the various differencing schemes, on the different meshes. A reference value for the vortex dimension ($x_{1,\mathrm{ref}}$), representative of the 'true' solution, and the observed order of accuracy (n) were calculated by a Richardson extrapolation-like technique. It was based on the following asymptotic relationship between the calculated primary-vortex length x_1 and the smallest cell size on a given mesh, $\Delta x_{\min}$:

$$x_1 = x_{1,\mathrm{ref}} + a(\Delta x_{\min})^n \tag{22}$$

With the results obtained on the finest meshes given in Table II, a non-linear regression allowed us to obtain the convergence-related parameters ($x_{1,\mathrm{ref}}$ and n) shown at the bottom of the table. Due to grid-nonuniformity and the effect of the other terms in the equations, the order of accuracy of the CUBISTA scheme is somewhat above 2. Both the results in Table II and the asymptotic error variation in Figure 14 show that, in terms of accuracy, the CUBISTA, SMART and WACEB schemes are equivalent. In terms of robustness, as seen beforehand, CUBISTA and WACEB are superior to SMART. The CLAM, GAMMA and MINMOD schemes, in comparison, show only a slight reduction in the order of accuracy, but the true errors are larger, especially for MINMOD. For example, on the second mesh (102×40), which represents a typical mesh to be used in practice, the recirculation length predicted by MINMOD has an error of 8.8%, and CLAM 4.9%, compared to 3.3% of CUBISTA. It is interesting to notice, from Figure 12, that MINMOD takes longer to converge than CUBISTA or WACEB. The GAMMA scheme, which was developed for unstructured mesh applications and so relies on interpolation between only the two nodes straddling a given cell face, shows very good results and is a good option for Newtonian flow calculations in complex geometries. The UDS is highly inaccurate, due to its first-order accuracy, and therefore should be avoided.

As an additional accuracy check of the present scheme, we give in Table III the various predicted recirculation lengths for the same problem but with inlet condition (ii), together with results from other sources. There is excellent agreement with the benchmark solution

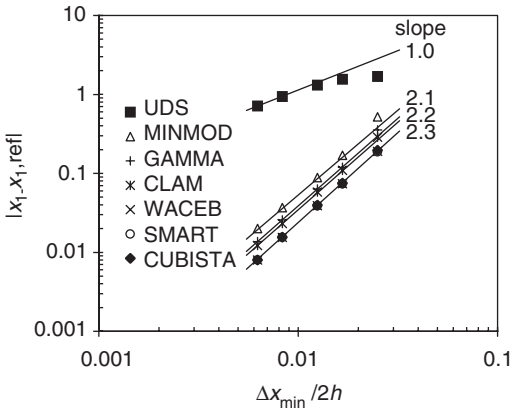

Figure 14. Estimated error in the primary-vortex dimension versus minimum cell size.

Table III. Reattachment and separation positions for the benchmark backward-facing step flow (no inlet channel).

	$x_1/2h$	$x_2/2h$	$x_3/2h$	$x_4/2h$	$y_4/2h$
This work	6.095	4.852	10.481	0.0864	0.0829
Gresho *et al.* [27]	6.10	4.85	10.48	n.a.*	n.a.*
Barton [28]	6.02	4.82	10.48	n.a.*	n.a.*

*Not available.

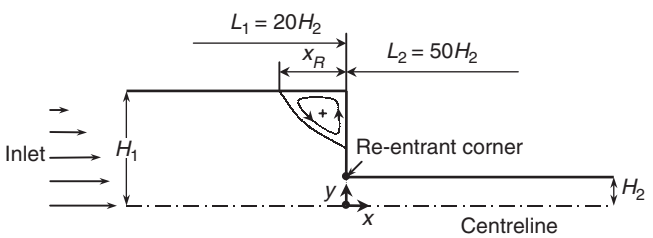

Figure 15. Geometry of the 4:1 planar contraction.

of Gresho *et al.* [27] based on a high-order finite element method, thus confirming the good level of accuracy achieved with the CUBISTA scheme.

5.3. Simulation of viscoelastic flows

We turn now to the final, but more complicated case of the flow of a viscoelastic UCM fluid, for which a clearer distinction among the schemes is going to emerge. We consider two problems: the first is the popular benchmark problem of the flow through a 4:1 planar contraction sketched in Figure 15 where the co-ordinate system and some of the relevant

dimensions are shown. The flow domain was mapped with orthogonal but non-uniform computational meshes, having increased concentration of cells near the re-entrant corner and along the downstream channel wall, where the highest stress gradients are observed. In previous work [15] it was found that a computational domain extending from $x = -20H_2$ to $x = +50H_2$ is sufficiently long to avoid end effects. This problem is characterized by a Reynolds number $Re \equiv \rho U_2 H_2/\eta = 0.01$, representative of slow-moving polymer melts, and a Deborah number $De \equiv \lambda U_2/H_2 \equiv 3$, representative of moderate to high viscoelastic flow. The fluid can be better characterized by an elasticity number defined as $E = De/Re$, giving $E = 300$ in the present situation and thus indicating a highly elastic fluid.

We have studied this problem in detail [15] using very refined meshes (up to 57 032 cells) in conjunction with the MINMOD scheme, and fairly accurate solutions could be obtained for Deborah numbers up to $De = 3$. Those solutions have been recently used by others [29] as a check of their results. In the present work the goal is to study the convergence and accuracy properties of the proposed CUBISTA scheme and how it compares with other high-resolution schemes. This problem provides a stringent test for the high-resolution schemes due both to the hyperbolic nature of the stress equation (Equation (4)), and the singular-like re-entrant corner of the contraction geometry which generates very high stress levels (theoretically tending to infinity). As a consequence the question of boundedness is of paramount importance; high-order schemes without limiter functions, such as the basic QUICK scheme, simply result in too many under/overshoots, often leading to divergence of the time-advancement procedure.

Calculations have been carried out on two meshes, one with 3 598 cells (denoted M1) and the other with a doubled number of cells along each direction, giving 14 258 cells (denoted M2). The minimum non-dimensional cell size for these meshes is 0.02 and 0.01, respectively, for M1 and M2, and it corresponds to square cells adjacent to the re-entrant corner. The convergence behaviour of the various differencing schemes on mesh M1 is illustrated in Figure 16, where the time decay of the τ_{xx} residuals is plotted against the dimensionless time, defined as $T = tU_2/H_2$, for a time step of $\delta T = 0.01$. This figure shows that the MINMOD, GAMMA, WACEB and SMART schemes all exhibit convergence difficulties. In the case of the GAMMA scheme, convergence can be achieved when the scheme's parameter is raised to $\beta_m = 0.5$, a value in the upper limit of the range that guarantees good accuracy [20]. For this mesh, the CLAM and CUBISTA schemes show similar residual decay (convergence speed) and the UDS is, once again, a little faster in attaining full convergence in terms of vanishing residuals ($< 10^{-4}$). On the fine mesh (M2), on the other hand, we found that only the UDS and the CUBISTA schemes are able to achieve fully converged solutions, as shown by Figure 17. On this mesh, even the CLAM scheme, which was designed as a curved smooth line in the NVD in order to avoid the switching instability [17, 18], is unable to provide a solution converged to the prescribed tolerance.

In terms of accuracy, we present in Figure 18 the contour plot of the dimensionless first-normal stress difference obtained using the proposed scheme. In the same figure, contour plots for the more accurate (SMART) and less accurate (UDS) schemes are shown for comparison. Once more, it is difficult to visually distinguish stress contours with CUBISTA and SMART. Although the stress contours obtained with the upwind scheme do not seem too different in this figure, a close inspection shows significantly more diffused stresses especially in the region close to the re-entrant corner. As a consequence the resulting streamline patterns with UDS are grossly in error as shown in Figure 19, where they are compared with those of CUBISTA on the same mesh (M1) and with reference (mesh-independent) streamlines obtained on a

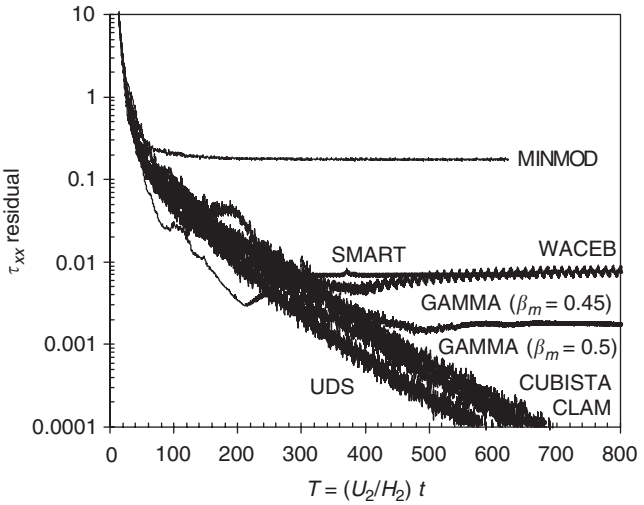

Figure 16. Decay of the norm of the τ_{xx} residuals for the various differencing schemes at $De = 3$. Results obtained on mesh M1.

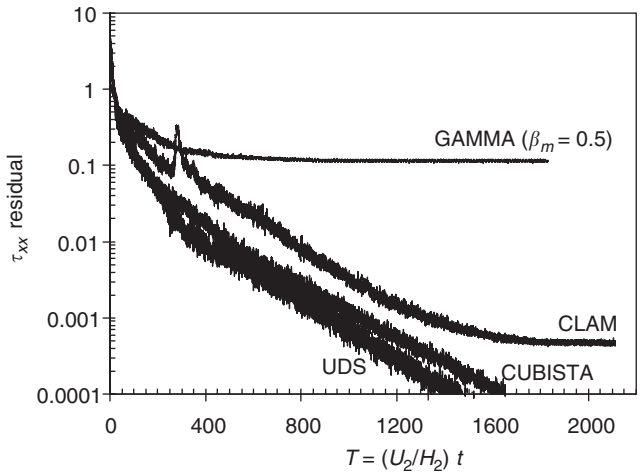

Figure 17. Decay of the norm of the τ_{xx} residuals for the UDS, GAMMA, CLAM and CUBISTA schemes at $De = 3$. Results obtained on mesh M2.

very fine mesh (with 57,032 control volumes, cf. Reference [15]). Clearly the CUBISTA streamlines on this rather coarse mesh M1 are close to the mesh-independent ones, while the upwind results exhibit an artificially enhanced corner vortex activity.

The second viscoelastic problem deals with the flow around a circular cylinder (radius R) placed in a channel (semi-width h; blockage $R/h = 0.5$), a relatively smooth flow (there is no singular point) but still difficult numerically due to the presence of steep stress boundary layers [16,30]. A sketch of the geometry is given in the inset of Figure 20, which shows the

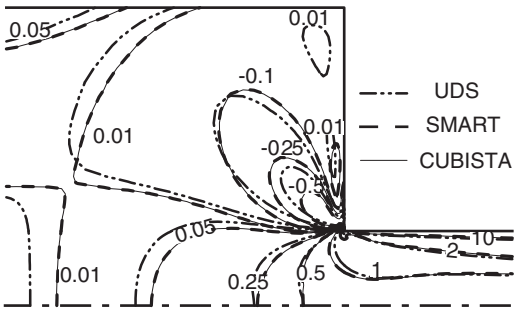

Figure 18. Contours of the first normal stress difference $(\tau_{xx}-\tau_{yy})/(3\eta U_2/H_2)$ obtained with the UDS, SMART and CUBISTA schemes on mesh M1.

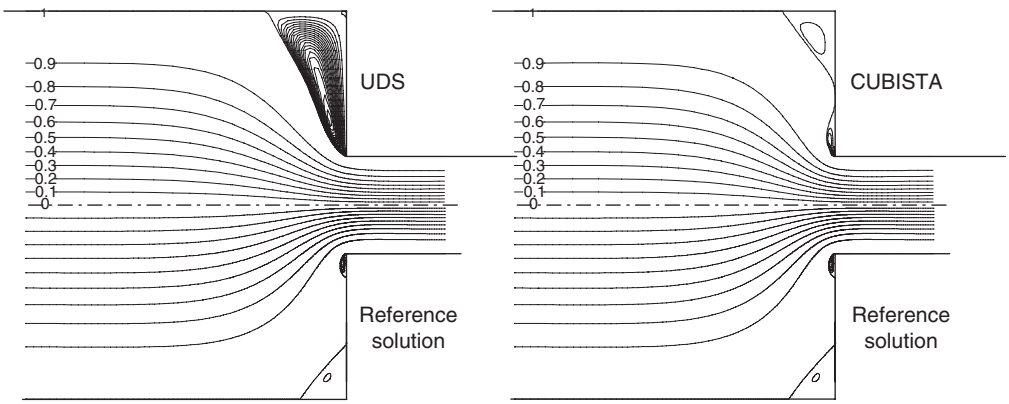

Figure 19. Effect of schemes' accuracy and numerical diffusion: comparison of streamlines (flow is left to right) predicted with UDS and CUBISTA on mesh M1 against a reference solution (Reference [15]: MINMOD on very fine mesh M4).

convergence behaviour of the various schemes at a Deborah number $De \equiv \lambda U/R = 0.6$, a value on the mid-range for this problem (both References [16] and [30] present a limiting $De \approx 1$). As in the previous problem, only upwind and the new scheme are capable of achieving converged results, approximately at the same convergence rate; MINMOD, SMART, WACEB and CLAM show a levelling out of the residuals decay, without iterative convergence. The time step used in these calculations was $\delta T = 0.002$ (normalized with R/U) and the mesh was that referred to as M30 in Reference [16], which is a relatively coarse mesh with 30 cells from the cylinder surface to the channel wall. A convenient solution functional for the assessment of numerical accuracy is the drag coefficient on the cylinder (C_d) which is given in Figure 21 as a function of the Deborah number. The present results with the CUBISTA and the upwind schemes on mesh M30 are compared with the Richardson-extrapolated mesh-independent solution of Reference [16] and results of Reference [30] who used an highly accurate h-p finite element method. The CUBISTA predictions of C_d on the relatively coarse mesh M30 follow the solution of both References [16] and [30] very well, up to $De = 0.9$,

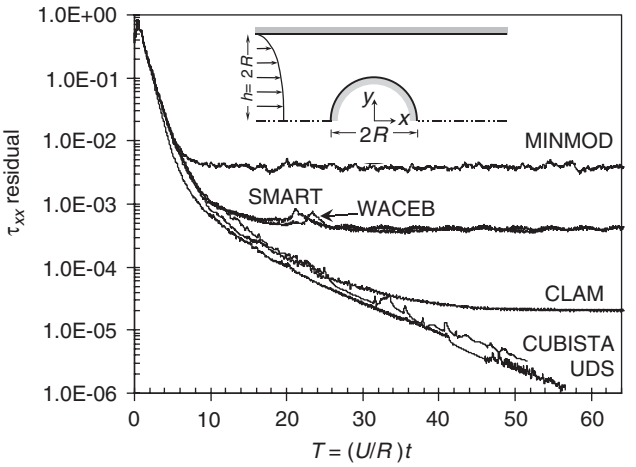

Figure 20. Iterative convergence behaviour of the various high resolution schemes for the cylinder problem ($De = 0.6$, mesh M30).

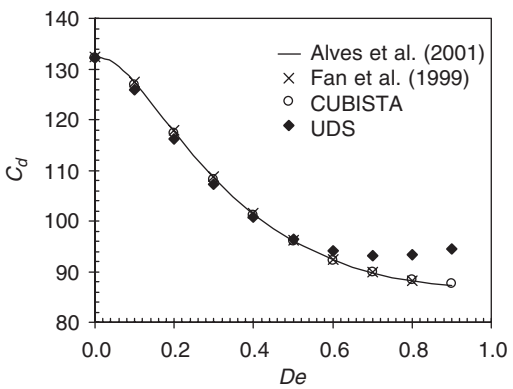

Figure 21. Comparison of the drag coefficient on the cylinder predicted with the new scheme (CUBISTA) and upwind (UDS) on mesh M30, against accurate results from References [16] and [30].

while the inaccuracies introduced by upwind on the stress predictions start deviating C_d from that solution for $De \geqslant 0.5$.

Some conclusive remarks regarding the above results are in order at this point. We see from Figures 16 and 20 that with MINMOD, which is known to be more diffusive than the other HRS's (e.g. Reference [12]), we cannot obtain a converged solution. The explanation must reside on the fact that the MINMOD characteristics in the NVD exhibit a change of slope at $\widehat{\phi}_P = 0.5$, in the smooth flow region, and therefore that scheme is more prone to the switching instability. SMART violates the TVD restrictions on both sides of the monotone region in the NVD, at $\widehat{\phi}_P \approx 0$ and 1, and so it will be subjected to convergence trouble whenever there are sharp up-gradients or down-gradients. This is why it requires some form of under-relaxation of

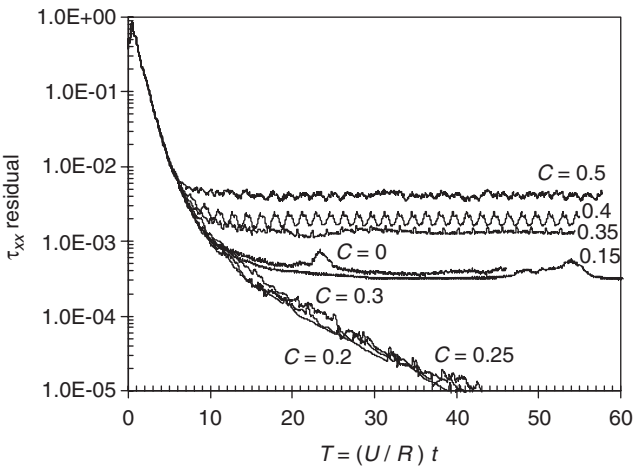

Figure 22. Effect of the parameter C on the convergence history for the problem of viscoelastic flow past a cylinder ($De = 0.6$; mesh M30).

the face fluxes [10, 17]. WACEB follows the steady-state TVD restrictions precisely ($C = 0$), but the results show (Figures 16 and 20) that such conditions are not sufficient to guarantee a converged solution: some safety margin is required, as in the CUBISTA scheme. This fact is especially important for situations in which $\widehat{\phi}_P \approx 1$, where the strict TVD constraints for $C = 0$ and the WACEB scheme follow the downwind scheme. Downwind differencing gives rise to a single negative coefficient in the linearized discrete equations, and that is highly unstable in conjunction with implicit solution methods. An interesting plot illustrating these remarks is provided by Figure 22 where the decay of τ_{xx} residuals with the elapsed time (proportional to the number of time steps) is shown for the cylinder problem at $De = 0.6$ for various values of the parameter C in the proposed scheme. For C in the range 0.2–0.3 good convergence is achieved, at approximately the same rate, thus confirming the good choice of the value $C = 0.25$ used in the CUBISTA scheme. For higher values of C ($C = 0.35$, 0.4 and 0.5) convergence cannot be achieved, in spite of the increased dissipation introduced. Note that $C = 0.5$ corresponds to the MINMOD scheme, and the switching instability in the smooth flow region must be the cause for lack of convergence seen in this range of C. For lower values of C ($C = 0$–0.15) convergence cannot again be achieved, this time because the TVD constraints (with finite C) are not satisfied.

6. CONCLUSIONS

A new high resolution scheme for the treatment of advected transport (named CUBISTA) is constructed in the context of the normalized variable and space formulation. It has similarly good accuracy as the well-known SMART scheme, but better iterative convergence properties when applied in an implicit solution method. This was achieved by incorporating total variation diminishing constraints into the design of the scheme. Assessment of the accuracy and convergence characteristics of the new scheme was carried out with a number of linear and

non-linear test cases involving both Newtonian and viscoelastic fluid flow. For the problem of Newtonian flow through a backward-facing step, the new scheme converged equally well as most of the other known high resolution schemes, with the exception of SMART which required smaller time steps. However, for the viscoelastic flow problems, which were the main motivation of this work, the new scheme was the only one to converge, either on a fine mesh or at all, of all the tested high resolution schemes. The relevance of this finding and of the new scheme can be better appreciated from knowledge that in order to predict accurately viscoelastic flows, very fine meshes are required [16].

ACKNOWLEDGEMENTS

M. A. Alves wishes to thank Universidade do Porto and his colleagues at Departamento de Engenharia Química for a temporary leave of absence, and acknowledges the Financial support of Fundação Calouste Gulbenkian.

REFERENCES

1. Leonard BP. Why you should not use 'hybrid' 'power-law' or related exponential schemes for convective modelling—there are much better alternatives. *International Journal for Numerical Methods in Fluids* 1995; **20**:421–442.
2. Patankar SV. *Numerical Heat Transfer and Fluid Flow*. Hemisphere: Washington, DC, 1980.
3. Spalding DB. A novel finite-difference formulation for differential expressions involving both first and second derivatives. *International Journal for Numerical Methods in Engineering* 1972; **4**:551–559.
4. Shyy W, Thakur S, Wright J. Second-order upwind and central difference schemes for recirculating flow computation. *AIAA Journal* 1992; **30**:923–932.
5. Leonard BP. A stable and accurate convective modelling procedure based on quadratic interpolation. *Computer Methods in Applied Mechanics and Engineering* 1979; **19**:59–98.
6. Hayase T, Humphrey JAC, Greif R. A consistently formulated QUICK scheme for fast and stable convergence using finite-volume iterative calculation procedures. *Journal of Computational Physics* 1992; **98**:108–118.
7. Harten A. High resolution schemes for hyperbolic conservation laws. *Journal of Computational Physics* 1983; **49**:357–393.
8. Sweby PK. High resolution schemes using flux limiters for hyperbolic conservation laws. *SIAM Journal on Numerical Analysis* 1984; **21**:995–1011.
9. Van Leer B. Towards the ultimate conservative difference scheme. II. Monotonicity and conservation combined in a second-order scheme. *Journal of Computational Physics* 1974; **14**:361–370.
10. Gaskell PH, Lau AKC. Curvature compensated convective transport: SMART, a new boundedness preserving transport algorithm. *International Journal for Numerical Methods in Fluids* 1988; **8**:617–641.
11. Leonard BP. Simple high-accuracy resolution program for convective modelling of discontinuities. *International Journal for Numerical Methods in Fluids* 1988; **8**:1291–1318.
12. Leonard BP. The ULTIMATE conservative difference scheme applied to unsteady one-dimensional advection. *Computer Methods in Applied Mechanics and Engineering* 1991; **88**:17–74.
13. Leonard BP. Bounded higher-order upwind multidimensional finite-volume convection-diffusion algorithms. In *Advances in Numerical Heat Transfer*, Minkowycz WJ, Sparrow EM (eds), vol. 1. Taylor and Francis: London, 1996; 1–57.
14. Darwish MS, Moukalled F. Normalized variable and space formulation methodology for high-resolution schemes. *Numerical Heat Transfer*, *Part B* 1994; **26**:79–96.
15. Alves MA, Pinho FT, Oliveira PJ. Effect of a high-resolution differencing scheme on finite-volume predictions of viscoelastic flows. *Journal of Non-Newtonian Fluid Mechanics* 2000; **93**:287–314.
16. Alves MA, Pinho FT, Oliveira PJ. The flow of viscoelastic fluids past a cylinder: finite-volume high-resolution methods. *Journal of Non-Newtonian Fluid Mechanics* 2001; **97**:207–232.
17. Zhu J. On the higher-order bounded discretization schemes for finite volume computations of incompressible flows. *Computer Methods in Applied Mechanics and Engineering* 1992; **98**:345–360.
18. Choi SK, Nam HY, Cho M. A comparison of higher-order bounded convection schemes. *Computer Methods in Applied Mechanics and Engineering* 1995; **121**:281–301.
19. Song B, Liu GR, Lam KY, Amano RS. On a higher-order bounded discretization scheme. *International Journal for Numerical Methods in Fluids* 2000; **32**:881–897.

20. Jasak H, Weller HG, Gosman AD. High resolution NVD differencing scheme for arbitrarily unstructured meshes. *International Journal for Numerical Methods in Fluids* 1999; **31**:431–449.
21. Bird RB, Armstrong RC, Hassager O. *Dynamics of Polymeric Liquids* (2nd edn.). Wiley: New York, 1987.
22. Baaijens FPT. Mixed finite element methods for viscoelastic flow analysis: a review. *Journal of Non-Newtonian Fluid Mechanics* 1998; **79**:361–385.
23. Oliveira PJ, Pinho FT, Pinto GA. Numerical simulation of non-linear elastic flows with a general collocated finite-volume method. *Journal of Non-Newtonian Fluid Mechanics* 1998; **79**:1–43.
24. Khosla PK, Rubin SG. A diagonally dominant second-order accurate implicit scheme. *Computers and Fluids* 1974; **2**:207–209.
25. Darwish MS, Moukalled F. The normalized weighting factor method: a novel technique for accelerating the convergence of high-resolution convective schemes. *Numerical Heat Transfer*, *Part* B 1996; **30**:217–237.
26. Hirsch C. *Numerical Computation of Internal and External Flows*, vol. 2. Wiley: New York, 1990.
27. Gresho PM, Gartling DK, Torczynki JR, Cliffe KA, Winters KH, Garrat TJ, Spence A, Goodrich JW. Is the steady viscous incompressible two-dimensional flow over a backward-facing step at $Re = 800$ stable? *International Journal for Numerical Methods in Fluids* 1993; **17**:501–541.
28. Barton IE. Comparison of SIMPLE and PISO type schemes for transient flows. *International Journal for Numerical Methods in Fluids* 1998; **26**:459–483.
29. Aboubacar M, Webster MF. A cell-vertex finite volume/element method on triangles for abrupt contraction viscoelastic flows. *Journal of Non-Newtonian Fluid Mechanics* 2001; **98**:83–106.
30. Fan Y, Tanner RI, Phan-Thien N. Galerkin/least-square finite-element methods for steady viscoelastic flows. *Journal of Non-Newtonian Fluid Mechanics* 1999; **84**:233–256.

